J. Fluid Mech. (1982), *vol.* 115, *pp.* 505–523
Printed in Great Britain

An infinite-series solution for the creeping motion through an orifice of finite length

By ZEEV DAGAN, SHELDON WEINBAUM AND ROBERT PFEFFER

The City College of The City University of New York, New York

(Received 1 December 1980 and in revised form 4 June 1981)

This paper presents an infinite-series solution to the creeping viscous motion of a fluid through low- and moderate-aspect-ratio pores. The flow field is divided into two simply bounded regions: a cylindrical volume bounded by the walls of the pore and the entrance and exit planes, and an infinite half-space outside the pore. Analytic solutions are first obtained in each region for unknown functions representing arbitrary axial and radial velocity profiles at the pore entrance (exit). These unknown functions are then determined by matching the normal and tangential stress at the pore opening.

The results indicate that the velocity profile approaches to within 1·5 per cent of a Poiseuille profile after a short entrance distance of half the pore radius. In the far field the solution matches exactly the streamline pattern for a flow through an orifice of zero thickness obtained by Sampson (1891). The pressure drop across the pore exhibits linear dependence on the aspect ratio and is closely approximated (less than one per cent error) by a simple algebraic expression.

1. Introduction

The creeping flow through a pore of finite length, including entrance and exit effects, has important applications to transport and filtration processes in biological and synthetic membranes. Some salient examples involving such motion include filtration of particle contaminants and aerosols, the molecular-sieving effects that are known to occur at the entrance of the so-called 'small pores' in biological membranes, the diffusion of macromolecules through vesicle attachment stalks in endothelial cell layers (Weinbaum & Caro 1976) and the Fahraeus–Lindqvist effect in blood capillaries (Fahraeus 1929; Fahraeus & Lindqvist 1931).

While boundary collocation (Gluckman, Pfeffer & Weinbaum 1971; Leichtberg, Pfeffer & Weinbaum 1976; Ganatos, Weinbaum & Pfeffer, 1980) and finite-element methods (Skalak, Chen & Chien 1972) have been applied with considerable success to internal flows in infinitely long tubes and external flows past more general boundary shapes, there are no existing solutions for the creeping motion through finite-length pores or the motion of a particle through an orifice or a finite-length pore. These effects are believed to have an important influence at low Reynolds numbers, where the influence of the boundaries decays algebraically. Existing analytic solutions have been limited to either the slow flow in an infinite half-space for an arbitrary prescribed velocity at the pore exit (Parmet & Saibel 1965) or the classic solution of Sampson (1891) for the flow through a circular hole in a zero-thickness plane wall. A number of

studies have also examined the locally valid two-dimensional flow near a sharp corner (Dean & Montagnon 1949; Lugt & Schwiderski 1965; Weinbaum 1968). The more difficult problem of determining the interaction between the flow inside and outside the pore was attempted by Weil & Schenectady (1951) for the two-dimensional counterpart of the present study: the Stokes jet exiting a slit into a half-space. These authors did not provide sufficient matching conditions to determine uniquely the flow field: only the velocity was matched and not the normal and tangential components of the viscous-stress tensor.

Weinbaum (1968) demonstrated the importance of the upstream influence on the pressure field and velocity profile for flow approaching the trailing edge of a blunt-base body. If upstream influence is neglected and a Blasius boundary-layer profile assumed just upstream of the corner, the pressure field corresponding to this solution cannot be matched with the uniform pressure field of the Blasius solution and an erroneous velocity field is predicted with separation occurring at the trailing edge. Similarly, the assumption that the flow inside the pore is fully developed and has a Poiseuille profile (Manton 1978) excludes the upstream influence in the pressure field across the edge of the orifice. Owing to the difficulty of analytically treating a three-dimensional corner flow interaction, several investigators have recently undertaken finite-difference Navier–Stokes solutions for representative pore geometries (Kanaoka, Emi & Nskada 1974; Smith & Phillips 1975; Parker & Buzzard 1978). However, the finite-difference method is limited owing to the admissibility of a weak singularity in the pressure field at the edge of the orifice. The locally singular shear stress prevents accurate numerical description of the pressure field because of the mesh-size limitation.

The problem of creeping flow through a finite-length orifice has eluded exact theoretical treatment because there is no natural co-ordinate system which can be used to satisfy the no-slip boundary conditions simultaneously inside on the orifice walls and outside on the wall which lies in the plane of the entrance or exit. The purpose of the present paper is to develop an efficient matching technique which could be used to treat an important class of previously unsolved axisymmetric creeping-motion problems where the general flow field can be divided into a set of simply bounded fields which cover the original flow field geometrically. Thus, the partitioning of a complex field may establish well-defined regions in which the solution for the velocity distribution is unique. One first satisfies the kinematic boundary conditions on the velocity in each region independently by prescribing in a general form the unknown velocity profile at the interface between any two adjacent regions. For a finite interface one chooses a convenient series representation with unknown coefficients. Hence, in each region one has a well-posed boundary-value problem which will admit a unique solution in terms of the unknown velocity at the interface with an adjacent region. This procedure assures continuity of the velocity field without accounting for the influence of the pressure field across the interfacial surfaces. In order to satisfy continuity of the pressure field, the normal and tangential stress at each interface have to be matched. This dynamic matching condition can be used to solve for the unknown coefficients in the general series representation of the local velocity profile. The method can also be applied to problems which include finite particles by making use of the collocation technique, described by Ganatos, Pfeffer & Weinbaum (1978), to satisfy the no-slip boundary conditions on finite closed surfaces. This extension of the technique to a sphere approaching an orifice or a disk is described in Dagan, Weinbaum &

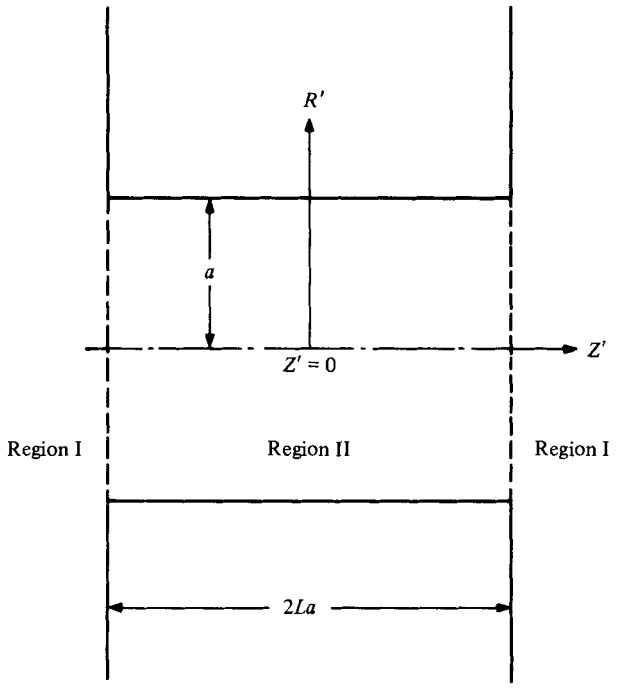

FIGURE 1. Geometry of an orifice of finite length and diameter.

Pfeffer (1981). Section 2 contains the mathematical formulation of the problem at hand for a pore of arbitrary dimensions and a prescribed pressure drop across the orifice. In § 3 the solution, obtained by the new technique, is presented and the far-field solution compared to Sampson's (1891) solution for the zero-thickness orifice. In addition, a simple expression is derived for the pressure drop across the orifice. Finally, in § 4 the extension of the present method to more general external flows past arbitrary boundary shapes is discussed.

2. Formulation for the creeping flow through a pore

The flow of interest is axisymmetric, so that the Stokes stream function can be used. It is convenient to formulate the problem in terms of dimensionless (unprimed) co-ordinates which are defined in terms of dimensional (primed) co-ordinates (figure 1) by

$$R = R'/a, \quad Z = Z'/a, \tag{2.1}$$

where a is the radius of the pore and (R', Z') are the cylindrical co-ordinates. The dependent variables are expressed in dimensionless form, using fluid density ρ, the kinematic viscosity ν and the pore radius a as follows:

$$\psi = \frac{\psi'}{a\nu}, \quad P = \frac{P'a^2}{\rho\nu^2}, \tag{2.2}$$

where ψ' is the stream function and P' is the pressure.

By omitting the inertial terms from the steady-state Navier–Stokes equations and introducing the axisymmetric stream function, the following equation is obtained:

$$D^2(D^2\psi) = 0, \tag{2.3a}$$

where D^2 is the generalized axisymmetric Stokesian operator, given by

$$D^2 = \frac{\partial^2}{\partial R^2} - \frac{1}{R}\frac{\partial}{\partial R} + \frac{\partial^2}{\partial Z^2}, \tag{2.3b}$$

and the velocity components in the axial and radial directions are

$$U_Z = \frac{1}{R}\frac{\partial\psi}{\partial R}, \quad U_R = -\frac{1}{R}\frac{\partial\psi}{\partial Z}. \tag{2.4a, b}$$

In accord with the comments in § 1, we divide the flow field into two simply bounded regions: a cylindrical volume bounded by the walls of the pore of the exit plane and the symmetry plane at $Z = 0$, and an infinite half-space outside the pore. Solutions to (2.3a) which are suitable for representing an arbitrary disturbance generated by the wall at $Z = L$ and which yield a finite velocity everywhere in the outer region are given by Parmet & Saibel (1965) in the form

$$\psi^{\mathrm{I}}(R,Z) = \int_0^\infty RJ_1(\omega R)\,[A(\omega) + ZB(\omega)]\,e^{-\omega Z}\,d\omega \quad (Z \geqslant L), \tag{2.5}$$

where $A(\omega)$ and $B(\omega)$ are unknown functions of ω, J_1 is the ordinary Bessel function of the first kind and L is the aspect ratio, or the dimensionless pore length. Inside the pore a symmetric solution about $Z = 0$, which generates finite velocities at $R = 0$, is constructed by superimposing the disturbances from the cylindrical boundary $R = 1$ given by Haberman & Sayre (1958), the vertical plane $Z = 0$ and the unknown flow that must match the solution in the infinite half-space $Z \geqslant L$:

$$\begin{aligned}\psi^{\mathrm{II}}(R,Z) = {} & C_0R^4 + D_0R^2 + \sum_{n=1}^{\infty}\,[C_nRI_1(\alpha_nR) + D_nR^2I_0(\alpha_nR)]\cos\alpha_nZ \\ & + \sum_{n=1}^{\infty}\,[F_nZ\sinh(\lambda_{n,1}Z) + G_n\cosh(\lambda_{n,1}Z)]\,RJ_1(\lambda_{n,1}R) \quad (0 \leqslant Z \leqslant L),\end{aligned} \tag{2.6}$$

where $C_0, D_0, C_n, \ldots, G_n$ are unknown constant coefficients, I_0 and I_1 are modified Bessel functions of the first kind, $\lambda_{n,\nu}$ are the zeros of J_ν, and $\alpha_n = n\pi/L$.

The kinematic solution for each region can now be obtained independently, provided the velocity at the exit of the pore is specified. This velocity, at the pore opening, is prescribed in a general form by a Fourier–Bessel series as follows:

$$\mathbf{U}(R,L) = \frac{f(R)}{R}\hat{\mathbf{z}} - \frac{g(R)}{R}\hat{\mathbf{r}} = \sum_{n=1}^{\infty}\,[a_nJ_0(\lambda_{n,0}R)\hat{\mathbf{z}} - b_nJ_1(\lambda_{n,1}R)\hat{\mathbf{r}}], \tag{2.7}$$

where $f(R)/R$ and $-g(R)/R$ are the axial and radial velocity components at $Z = L$ and $R \leqslant 1$, respectively, and a_n and b_n are unknown constant coefficients.

Using the definition (2.7) for the exit velocity, the no-slip boundary conditions on the wall $Z = L$ are

$$U_Z^{\mathrm{I}}(R,L) = \frac{1}{R}\frac{\partial\psi^{\mathrm{I}}}{\partial R}(R,L) = F(R) = \begin{cases} 0 & (R > 1), \\ f(R)/R & (0 < R < 1), \end{cases} \tag{2.8a}$$

$$U_R^{\mathrm{I}}(R,L) = -\frac{1}{R}\frac{\partial\psi^{\mathrm{I}}}{\partial Z}(R,L) = G(R) = \begin{cases} 0 & (R > 1), \\ -g(R)/R & (0 < R < 1), \end{cases} \tag{2.8b}$$

while (2.7) and the no-slip boundary conditions

$$U_Z^{\mathrm{II}}(1,Z) = \frac{1}{R}\frac{\partial \psi^{\mathrm{II}}}{\partial R}(1,Z) = 0 \quad (0 \leqslant Z \leqslant L), \tag{2.9a}$$

$$U_R^{\mathrm{II}}(1,Z) = -\frac{1}{R}\frac{\partial \psi^{\mathrm{II}}}{\partial Z}(1,Z) = 0 \quad (0 \leqslant Z \leqslant L), \tag{2.9b}$$

have to be satisfied in the inner region.

Finally, the shear-stress matching condition at $Z = L$ and $0 \leqslant R \leqslant 1$ requires

$$\tau_{ij}^{\mathrm{I}} = \tau_{ij}^{\mathrm{II}} \tag{2.10}$$

where τ_{ij} is the stress tensor.

Application of the boundary conditions (2.8*a*, *b*) along the wall $Z = L$ results in

$$\int_0^\infty \omega J_0(\omega R)\, F^*(\omega, L)\, d\omega = F(R), \tag{2.11a}$$

$$-\int_0^\infty \omega J_1(\omega R)\, G^*(\omega, L)\, d\omega = G(R), \tag{2.11b}$$

where

$$F^*(\omega, Z) = [A(\omega) + ZB(\omega)]\, e^{-\omega Z}, \tag{2.12a}$$

$$G^*(\omega, Z) = \frac{1}{\omega}[(1-\omega Z)\, B(\omega) - A(\omega)]\, e^{-\omega Z}. \tag{2.12b}$$

The right-hand sides of (2.11) represent the disturbances produced by the plane $Z = L$, and propagate downstream. These disturbances are functions only of the radial co-ordinate R. Inspection of (2.11) shows that the unknown functions F^* and G^*, evaluated at the plane of the opening, are simply Hankel transforms of these disturbances. The equations may be inverted to give

$$F^*(\omega, L) = \int_0^1 f(\xi)\, J_0(\omega\xi)\, d\xi, \tag{2.13a}$$

$$G^*(\omega, L) = \int_0^1 g(\xi)\, J_1(\omega\xi)\, d\xi. \tag{2.13b}$$

Equations (2.13) give the F^* and G^* functions evaluated at $Z = L$ in terms of the as yet unknown velocity components at the pore exit. To obtain these functions at any value of Z one must determine the unknown functions $A(\omega)$ and $B(\omega)$ in (2.12). The expressions for F^* and G^* obtained from (2.13) are substituted into (2.12), whose right-hand sides are evaluated at the plane $Z = L$. This gives rise to two linear algebraic equations, which may be solved simultaneously to yield the unknown functions $A(\omega)$ and $B(\omega)$. Once these functions are obtained, they are substituted back into (2.12) to give the F^* and G^* functions at any value of Z. The resulting expressions are

$$F^*(\omega, Z) = \left\{[1+\omega(Z-L)]\int_0^1 f(\xi)\, J_0(\omega\xi)\, d\xi + (Z-L)\int_0^1 g(\xi)\, J_1(\omega\xi)\, d\xi\right\} e^{-\omega(Z-L)}, \tag{2.14a}$$

$$G^*(\omega, Z) = -\left\{(Z-L)\int_0^1 f(\xi)\, J_0(\omega\xi)\, d\xi - [1-\omega(Z-L)]\int_0^1 g(\xi)\, J_1(\omega\xi)\, d\xi\right\} e^{-\omega(Z-L)}. \tag{2.14b}$$

Using the definition of the stream function, one can write the local fluid velocity at any point in the outer region as a function of the Hankel transforms of F^* and G^*,

which in turn are functions of the unknown velocity components f and g at the pore exit:

$$U_Z^{\mathrm{I}}(R,Z) = \int_0^\infty \omega F^*(\omega,Z)\,J_0(\omega R)\,d\omega, \tag{2.15a}$$

$$U_R^{\mathrm{I}}(R,Z) = -\int_0^\infty \omega G^*(\omega,Z)\,J_1(\omega R)\,d\omega, \tag{2.15b}$$

where from (2.5) the expression for the stream function in the outer region is given by

$$\psi^{\mathrm{I}}(R,Z) = \int_0^\infty RF^*(\omega,Z)\,J_1(\omega R)\,d\omega. \tag{2.16}$$

The solution (2.16) satisfies the no-slip boundary conditions along the wall at the plane of the opening for any arbitrary axisymmetric velocity profile at the pore exit.

The boundary conditions to be satisfied in the inner region at $R = 1$ and at $Z = L$ are most conveniently applied by using the series representation of the exit velocity rather than the f and g functions. At $R = 1$ the no-slip boundary conditions (2.8) require that:

$$4C_0 + 2D_0 + \sum_{n=1}^{\infty} \{C_n\alpha_n I_0(\alpha_n) + D_n[2I_0(\alpha_n) + \alpha_n I_1(\alpha_n)]\}\cos\alpha_n Z$$
$$= -\sum_{n=1}^{\infty} [F_n Z\sinh(\lambda_{n,1}Z) + G_n\cosh(\lambda_{n,1}Z)]\,\lambda_{n,1}J_0(\lambda_{n,1}), \tag{2.17a}$$

$$\sum_{n=1}^{\infty} [C_n I_1(\alpha_n) + D_n I_0(\alpha_n)]\sin\alpha_n Z = 0. \tag{2.17b}$$

The left-hand sides of (2.17) are simply the Fourier-series representations of the right-hand sides on the interval $[0, L]$. They may be inverted to give

$$4C_0 + 2D_0 = -\frac{1}{L}\sum_{n=1}^{\infty}\left\{F_n\left[L\cosh(\lambda_{n,1}L) - \frac{1}{\lambda_{n,1}}\sinh(\lambda_{n,1}L)\right] + G_n\sinh(\lambda_{n,1}L)\right\}J_0(\lambda_{n,1}), \tag{2.18a}$$

$$C_p\alpha_p I_0(\alpha_p) + D_p[2I_0(\alpha_p) + \alpha_p I_1(\alpha_p)]$$
$$= (-1)^{p+1}\frac{2}{L}\sum_{n=1}^{\infty}\left\{F_n\left[\lambda_{n,1}L\cosh(\lambda_{n,1}L) - \frac{\lambda_{n,1}^2 - \alpha_p^2}{\lambda_{n,1}^2 + \alpha_p^2}\sinh(\lambda_{n,1}L)\right]\right.$$
$$\left. + G_n(\lambda_{n,1}\sinh(\lambda_{n,1}L)\right\}\frac{\lambda_{n,1}J_0(\lambda_{n,1})}{\lambda_{n,1}^2 + \alpha_p^2}, \tag{2.18b}$$

$$C_n I_1(\alpha_n) + D_n I_0(\alpha_n) = 0. \tag{2.18c}$$

At the pore exit the solution must satisfy the arbitrary velocity profile (2.7). Using the expression for the stream function in the inner region, (2.6), we require that

$$2D_0 + \sum_{n=1}^{\infty} F_n L\sinh(\lambda_{n,1}L) + G_n\cosh(\lambda_{n,1}L)]\,\lambda_{n,1}J_0(\lambda_{n,1}R)$$
$$= -4C_0R^2 - \sum_{n=1}^{\infty}(-1)^n\{C_n\alpha_n I_0(\alpha_n R) + D_n[2I_0(\alpha_n R) + \alpha_n R I_1(\alpha_n R)]\}$$
$$+ \sum_{n=1}^{\infty} a_n J_0(\lambda_{n,0}R) \quad (0 \leqslant R \leqslant 1), \tag{2.19a}$$

$$\sum_{n=1}^{\infty}\{F_n[\lambda_{n,1}L\cosh(\lambda_{n,1}L) + \sinh(\lambda_{n,1}L)] + G_n\lambda_{n,1}\sinh(\lambda_{n,1}L)\}J_1(\lambda_{n,1}R)$$
$$= \sum_{n=1}^{\infty} b_n J_1(\lambda_{n,1}R) \quad (0 \leqslant R \leqslant 1). \tag{2.19b}$$

Here the disturbance from the outer region at the pore exit is represented by the Fourier–Bessel series expressing the exit-velocity components. The left-hand side is observed to be a Dini-series representation of the right-hand side in (2.19*a*), while in (2.19*b*) it is a Fourier–Bessel representation of the right-hand side. Inversion of these together with (2.18*c*) yields the following relations:

$$C_0 + D_0 = \sum_{n=1}^{\infty} \frac{a_n J_1(\lambda_{n,0})}{\lambda_{n,0}}, \tag{2.20a}$$

$$[F_p L \sinh(\lambda_{p,1} L) + G_p \cosh(\lambda_{p,1} L)]\lambda_{p,1} J_0(\lambda_{p,1}) + \frac{16}{\lambda_{p,1}^2} C_0 + 4\lambda_{p,1}^2 \sum_{n=1}^{\infty} \frac{(-1)^n \alpha_n}{(\lambda_{p,1}^2 + \alpha_n^2)^2} I_1(\alpha_n) D_n = 2 \sum_{n=1}^{\infty} a_n \frac{J_1(\lambda_{n,0})\lambda_{n,0}}{\lambda_{n,0}^2 - \lambda_{p,1}^2}, \tag{2.20b}$$

$$F_n[\lambda_{n,1} L \cosh(\lambda_{n,1} L) + \sinh(\lambda_{n,1} L)] + G_n \lambda_{n,1} \sinh(\lambda_{n,1} L) = b_n. \tag{2.20c}$$

The kinematic solution for each region is now known in terms of the unknown velocity at the pore opening. The functions $A(\omega)$ and $B(\omega)$, introduced in the stream-function representation of the outer region, have been obtained in terms of the f and g functions (2.14), while the solution for the constant coefficients in the expression for the stream function in the inner region are known implicitly in terms of the constant coefficients in the series representation of the pore exit velocity (2.18), (2.20). However, these two solutions have been obtained without taking account of the upstream influence in the pressure field across the plane of the pore. It is this latter dynamic condition which we now use to determine a unique solution for $f(R)$ and $g(R)$.

The components of the stress tensor, to be matched at $Z = L$, can be written in the general dimensionless form:

$$\tau_{ij} n_j = (-\delta_{ij} P + 2e_{ij}) n_j, \tag{2.21}$$

where δ_{ij} is the Kronecker delta, P is the pressure, $2e_{ij}$ is the rate-of-strain tensor and n_j is the normal to the matching surface. Since the pressure in Stokes flow is a harmonic function it can be matched independently, leaving the normal and tangential components of e_{ij} to be matched. These components are given by

$$e_{ZZ} = \frac{\partial U_Z}{\partial Z}, \quad e_{RZ} = \frac{1}{2}\left(\frac{\partial U_Z}{\partial Z} + \frac{\partial U_R}{\partial Z}\right). \tag{2.22a, b}$$

Examination of (2.22) indicates that e_{ZZ} and $\partial U_Z/\partial R$ are continuous across the interface by virtue of the matched radial and axial velocity components. The matching of the remaining term $\partial U_Z/\partial R$ can be replaced by requiring a continuous pressure gradient. This condition is a consequence of the direct relations between the pressure gradient and the rate-of-strain tensor in steady creeping flow. Namely, at $Z = L$ we require that

$$P^{\mathrm{I}} = P^{\mathrm{II}} \quad (0 \leqslant R \leqslant 1), \tag{2.23a}$$

$$\frac{\partial P^{\mathrm{I}}}{\partial Z} = \frac{\partial P^{\mathrm{II}}}{\partial Z} \quad (0 \leqslant R \leqslant 1). \tag{2.23b}$$

The general relations between the pressure and the stream function in steady creeping flow may readily be established from the Navier–Stokes equations. In dimensionless form these relations are

$$\frac{\partial P}{\partial Z} = \frac{1}{R}\frac{\partial}{\partial R}(D^2\psi), \tag{2.24a}$$

$$\frac{\partial P}{\partial R} = -\frac{1}{R}\frac{\partial}{\partial Z}(D^2\psi). \tag{2.24b}$$

The pressure field in each region is determined by integration of (2.24) with the appropriate stream-function representation. For the outer region the resulting equation is

$$P^{\mathrm{I}}(R,Z) = 2\int_0^\infty \omega J_0(\omega R)\, B(\omega)\, e^{-\omega Z}\, d\omega + P_\infty, \tag{2.25}$$

and for the inner region

$$P^{\mathrm{II}}(R,Z) = P_0 + 16C_0 Z + 2\sum_{n=1}^{\infty} D_n \alpha_n I_0(\alpha_n R)\sin \alpha_n Z + 2\sum_{n=1}^{\infty} F_n \lambda_{n,1} \sinh(\lambda_{n,1} L)\, J_0(\lambda_{n,1} R), \tag{2.26}$$

where P_0 is the uniform pressure at the plane of symmetry $Z = 0$, and P_∞ is the downstream pressure as $Z \to \infty$.

Introducing the expressions for the pressure, (2.25) and (2.26), into the matching condition (2.23), and substituting $B(\omega)$ from (2.12) and (2.14) yields the following coupled integral equations:

$$\int_0^\infty \omega^2 J_0(\omega R)\,[F^*(\omega, L) + G^*(\omega, L)]\, d\omega = \tfrac{1}{2}\overline{\Delta P} + 8LC_0 + \sum_{n=1}^{\infty} F_n \lambda_{n,1} \sinh(\lambda_{n,1} L)\, J_0(\lambda_{n,1} R) \quad (0 \leqslant R < 1), \tag{2.27a}$$

$$-\int_0^\infty \omega^3 J_0(\omega R)\,[F^*(\omega, L) + G^*(\omega, L)]\, d\omega = 8C_0 + \sum_{n=1}^{\infty} D_n (-1)^n \alpha_n^2 I_0(\alpha_n R) + \sum_{n=1}^{\infty} F_n \lambda_{n,1}^2 \cosh(\lambda_{n,1} L)\, J_0(\lambda_{n,1} R) \quad (0 \leqslant R < 1), \tag{2.27b}$$

where

$$\overline{\Delta P} = P_0 - P_\infty \tag{2.28}$$

is half the pressure drop across the pore.

The above integral equations, to the best of the authors' knowledge, cannot be solved explicitly for the F^* and G^* functions unless the behaviour of the integrals in (2.27) is specified for $R > 1$ (Tranter 1951). Clearly, such information cannot be provided because it requires knowledge of the solution for the pressure and its gradient along the exterior wall of the pore. Therefore it is advantageous to replace these functions by their appropriate series representations given by (2.7) and (2.13), and to determine the unknown coefficients a_n and b_n in the expansions. Furthermore, in order to eliminate the weak singularity in the pressure field, exhibited by the divergence of the integral expression at $R = 1$, the pressure is integrated over the area of a circle of radius R. The resulting conditions represent the matching of the force acting on the interface between the two regions and its gradient, which are analytic everywhere in the interval $0 \leqslant R \leqslant 1$. Following the outlined procedure, one obtains the equations

$$\sum_{n=1}^{\infty} a_n J_0(\lambda_{n,0} R) = a^*(R), \tag{2.29a}$$

$$\sum_{n=1}^{\infty} b_n J_1(\lambda_{n,1} R) = b^*(R), \tag{2.29b}$$

where

$$a^*(R) = \sum_{n=1}^{\infty} a_n + 2C_0R^2 + \sum_{n=1}^{\infty} D_n(-1)^n[I_0(\alpha_n R)-1] - \sum_{n=1}^{\infty} F_n \cosh(\lambda_{n,1}L)[J_0(\lambda_{n,1}R)-1]$$
$$- \sum_{n=1}^{\infty} b_n \int_0^{\infty} d\omega\, \omega[J_0(\omega R)-1] \int_0^1 d\xi\, \xi J_1(\lambda_{n,1}\xi) J_1(\omega\xi), \quad (2.30a)$$

$$b^*(R) = (4LC_0 + \tfrac{1}{4}\overline{\Delta P})R + \sum_{n=1}^{\infty} F_n \sinh(\lambda_{n,1}L) J_1(\lambda_{n,1}R)$$
$$- \sum_{n=1}^{\infty} a_n \int_0^{\infty} d\omega\, \omega J_1(\omega R) \int_0^1 d\xi\, \xi J_0(\lambda_{n,0}\xi) J_0(\omega\xi). \quad (2.30b)$$

Equations (2.29) are simply Fourier–Bessel series representations of the functions $a^*(R)$ and $b^*(R)$. A solution for a_n and b_n is readily available in the form

$$a_n = \frac{2}{J_1^2(\lambda_{n,0})} \int_0^1 t a^*(t) J_0(\lambda_{n,0}t)\, dt, \quad (2.31a)$$

$$b_n = \frac{2}{J_0^2(\lambda_{n,1})} \int_0^1 t b^*(t) J_1(\lambda_{n,1}t)\, dt. \quad (2.31b)$$

The integrals required in (2.31) are performed analytically (see appendix) resulting, after some rearrangement, in

$$b_n \frac{J_0(\lambda_{n,1})}{\lambda_{n,1}} + 2\sum_{k=1}^{\infty} a_k \lambda_{k,0} J_1(\lambda_{k,0}) A_{kn} - F_n \sinh(\lambda_{n,1}L) \frac{J_0(\lambda_{n,1})}{\lambda_{n,1}} + \frac{8LC_0}{\lambda_{n,1}^2} = -\frac{\overline{\Delta P}}{2\lambda_{n,1}^2}, \quad (2.32a)$$

$$a_n \frac{J_1(\lambda_{n,0})}{\lambda_{n,0}} - \frac{2}{\lambda_{n,0}^2} \sum_{k=1}^{\infty} a_k + 2\sum_{k=1}^{\infty} b_k \lambda_{k,1} J_0(\lambda_{k,1}) B_{kn}$$
$$+ 2\sum_{k=1}^{\infty} F_k \cosh(\lambda_{k,1}L) \left[\frac{J_0(\lambda_{k,1})}{\lambda_{n,0}^2 - \lambda_{k,1}^2} - \frac{1}{\lambda_{n,0}^2}\right]$$
$$- 2\sum_{k=1}^{\infty} D_k(-1)^k \left[\frac{I_0(\alpha_k)}{\alpha_k^2 + \lambda_{n,0}^2} - \frac{1}{\lambda_{n,0}^2}\right] - \frac{4C_0}{\lambda_{n,0}^2}\left(1 - \frac{4}{\lambda_{n,0}^2}\right) = 0, \quad (2.32b)$$

where

$$A_{kn} = \frac{S(\lambda_{k,0}) - S(\lambda_{n,1})}{\lambda_{k,0}^2 - \lambda_{n,1}^2}, \quad (2.33a)$$

$$B_{kn} = \frac{1}{\lambda_{n,0}^2}[\tfrac{1}{2}\pi H_1(\lambda_{k,1}) - 1] + A_{nk}, \quad (2.33b)$$

and the function $S(x)$ is given by

$$\frac{2}{\pi} + S(x) = \int_0^1 H_1(2x(1-t^2)^{\frac{1}{2}})\, dt = \frac{16x^2}{9\pi}\, {}_2F_3(2, 1; \tfrac{3}{2}, \tfrac{5}{2}, \tfrac{5}{2}; -x^2). \quad (2.34)$$

Here H_1 is the Struve function of order one, and ${}_2F_3$ is the generalized hypergeometric series.

Equations (2.18), (2.20) and (2.32) constitute the fundamental infinite set of linear algebraic equations for all six sets of unknown constant coefficients (C_n, D_n, F_n, G_n, a_n and b_n) and the constants C_0 and D_0. This set can be reduced, by a standard elimination procedure, to include only four sets of unknown coefficients (D_n, F_n, G_n and a_n) and the

constant C_0. In addition, it is advantageous, for the purpose of numerical computations, to define the unknown coefficients as follows:

$$\left.\begin{aligned} \bar{C}_n &= C_n I_1(\alpha_n), \quad \bar{D}_n = D_n I_0(\alpha_n), \\ \bar{F}_n &= F_n L \sinh(\lambda_{n,1} L), \quad \bar{G}_n = G_n \cosh(\lambda_{n,1} L). \end{aligned}\right\} \tag{2.35}$$

Consequently, the resulting system of equations is

$$8LC_0 + \sum_{i=1}^{\infty} a_i a_{ij}^{\mathrm{I}} + \bar{F}_j F_j^{\mathrm{I}} + \bar{G}_j G_j^{\mathrm{I}} = -\tfrac{1}{2}\overline{\Delta P}, \tag{2.36a}$$

$$16C_0 + \sum_{i=1}^{\infty} (a_i a_{ij}^{\mathrm{II}} + \bar{D}_i D_{ij}^{\mathrm{II}}) + \bar{F}_j F_j^{\mathrm{II}} + G_j \bar{G}_j^{\mathrm{II}} = 0, \tag{2.36b}$$

$$\bar{D}_j D_j^{\mathrm{III}} + \sum_{i=1}^{\infty} (\bar{F}_i F_{ij}^{\mathrm{III}} + \bar{G}_i G_{ij}^{\mathrm{III}}) = 0, \tag{2.36c}$$

$$C_{0j} C_0 + \sum_{i=1}^{\infty} (a_i a_{ij}^{\mathrm{IV}} + \bar{D}_i D_{ij}^{\mathrm{IV}} + \bar{F}_i F_{ij}^{\mathrm{IV}} + \bar{G}_i G_{ij}^{\mathrm{IV}}) = 0, \tag{2.36d}$$

$$2C_0 + \sum_{i=1}^{\infty} (a_i a_i^{\mathrm{V}} + \bar{F}_i F_i^{\mathrm{V}} + \bar{G}_i G_i^{\mathrm{V}}) = 0, \tag{2.36e}$$

where

$$a_{ij}^{\mathrm{I}} = 2\lambda_{i,0} J_1(\lambda_{i,0})\, A_{ij} \lambda_{j,1}^2, \quad F_j^{\mathrm{I}} = \lambda_{j,1}^2 \coth(\lambda_{j,1} L)\, J_0(\lambda_{j,1}), \tag{2.37a, b}$$

$$G_j^{\mathrm{I}} = \lambda_{j,1}^2 \tanh(\lambda_{j,1} L)\, J_0(\lambda_{j,1}), \quad a_{ij}^{\mathrm{II}} = -2J_1(\lambda_{i,0}) \frac{\lambda_{i,0} \lambda_{j,1}^2}{\lambda_{i,0}^2 - \lambda_{j,1}^2}, \tag{2.37c, d}$$

$$D_{ij}^{\mathrm{II}} = 4(-1)^i \frac{I_i(\alpha_i)}{I_0(\alpha_i)} \frac{\alpha_i \lambda_{j,1}^4}{(\alpha_i^2 + \lambda_{j,1}^2)^2}, \quad F_j^{\mathrm{II}} = G_j^{\mathrm{II}} = \lambda_{j,1}^3 J_0(\lambda_{j,1}), \tag{2.37e, f, g}$$

$$D_j^{\mathrm{III}} = \left[2 + \alpha_j \frac{I_1(\alpha_j)}{I_0(\alpha_j)} - \alpha_j \frac{I_0(\alpha_j)}{I_1(\alpha_j)}\right](-1)^j, \tag{2.37h}$$

$$F_{ij}^{\mathrm{III}} = \frac{2}{L^2} \frac{\lambda_{i,1} J_0(\lambda_{i,1})}{\alpha_j^2 + \lambda_{i,1}^2} \left[L\lambda_{i,1} \coth(\lambda_{i,1} L) + \frac{\alpha_j^2 - \lambda_{i,1}^2}{\alpha_j^2 + \lambda_{i,1}^2}\right], \tag{2.37i}$$

$$G_{ij}^{\mathrm{III}} = \frac{2}{L} \frac{\lambda_{i,1}^2 J_0(\lambda_{i,1})}{\alpha_j^2 + \lambda_{i,1}^2} \tanh(\lambda_{i,1} L), \quad a_{ij}^{\mathrm{IV}} = \delta_{ij} \frac{J_1(\lambda_{j,0})}{\lambda_{j,0}} - \frac{2}{\lambda_{j,0}}, \tag{2.37j, k}$$

$$D_{ij}^{\mathrm{IV}} = 2(-1)^{i+1} \left[\frac{1}{\alpha_i^2 + \lambda_{j,0}^2} - \frac{1}{I_0(\alpha_i)\, \lambda_{j,0}^2}\right], \tag{2.37l}$$

$$F_{ij}^{\mathrm{IV}} = 2\left\{\frac{1}{L} \coth(\lambda_{i,1} L) \left[\frac{J_0(\lambda_{i,1})}{\lambda_{j,0}^2 - \lambda_{i,1}^2} - \frac{1}{\lambda_{j,0}^2}\right] + \left[\lambda_{i,1} \coth(\lambda_{i,1} L) + \frac{1}{L}\right] \lambda_{i,1} J_0(\lambda_{i,1})\, B_{ij}\right\}, \tag{2.37m}$$

$$G_{ij}^{\mathrm{IV}} = 2 \tanh(\lambda_{i,1} L)\, \lambda_{i,1}^2 J_0(\lambda_{i,1})\, B_{ij}, \tag{2.37n}$$

$$a_i^{\mathrm{V}} = \frac{2}{\lambda_{i,0}} J_1(\lambda_{i,0}), \quad F_i^{\mathrm{V}} = \frac{1}{L} \left[\coth(\lambda_{i,1} L) - \frac{1}{L\lambda_{i,1}}\right] J_0(\lambda_{i,1}), \tag{2.37o, p}$$

$$G_i^{\mathrm{V}} = \frac{1}{L} \tanh(\lambda_{i,1} L)\, J_0(\lambda_{i,1}), \quad C_{0j} = -\frac{4}{\lambda_{j,0}^2} \left(1 - \frac{4}{\lambda_{j,0}^2}\right). \tag{2.37q, r}$$

The unknown constant coefficients in (2.36) can be evaluated numerically to any degree of accuracy by increasing the number of equations utilized.

3. Numerical results

Computations were performed on an AMDAHL/470/V6 computer. One first evaluates the coefficients C_0, a_n, $\bar{D}_n$, $\bar{F}_n$ and $\bar{G}_n$ by solving successively larger truncations of (2.36). Truncation after N terms requires a solution of $4N+1$ linear algebraic equations which yield the first N values of each set of coefficients and the constant C_0. Convergence of the results was tested by comparing the values of the volumetric flow rate Q, the constant C_0 and the centre-line velocity at the pore exit for various values of the aspect ratio L, and the number of coefficients N (figures 2(*a–c*)). Q was calculated by integrating the axial velocity at the pore exit over the area of the pore, while the centre-line velocity shown in figure 2(*c*) is simply the sum of the a_n coefficients obtained from the solution of (2.36). Figure 2 shows that for $L \sim O(1)$ the results change by less than 1 % as N increases from 20 to 100, and that the convergence of these results deteriorates as L approaches zero.

Values of the stream function ψ were computed next, for increasing values of N until they did not change in the first three significant figures. For $L = 1$, the value of the stream function was calculated from (2.6) (for the inner region) and (2.16) (for the outer region), using a grid of 10×10 points in each region, from which streamlines were drawn by interpolation (figure 3). The double integrals in (2.16) were calculated by analytically integrating the inner integrals and then using numerical integration to evaluate the remaining improper integrals. The pressure field in the inner region was calculated from (2.26) using a grid of 10×10 points. The pressure field in the outer region was computed from (2.25) using a similar grid except in the local region near the edge of the orifice, $0{\cdot}8 \leqslant Z \leqslant 1{\cdot}2$ and $0{\cdot}8 \leqslant R \leqslant 2$, where a finer grid of 40×120 points was used. The integration in (2.25) was performed in a similar manner to that described for the calculation of the stream function from (2.16). Lines of constant pressure were drawn by interpolation and are shown in figure 4. In figure 5 the pressure field near the edge of the orifice is compared to the locally valid two-dimensional solution obtained by Weinbaum (1968). Qualitatively the two fields exhibit similar behaviour with increasing resemblance as the length scale near the edge of the orifice is further magnified.

The streamline pattern shown in figure 3 for $L = 1$ is similar in the far field to the exact solution for the flow through a circular hole in a plane wall (Sampson 1891), while inside the pore the axial velocity approaches a Poiseuille profile with less than 1·5 % deviation after a short entrance distance equal to half the pore radius. The pressure field (figure 4) is also compatible with the far-field behaviour exhibited in Sampson's solution and approaches the linear axial-pressure-gradient behaviour associated with Poiseuille flow inside the pore.

Computations were carried out for various values of L between 0·25 and 2. When $L > \frac{1}{2}$ the flow inside the pore approaches Poiseuille flow in the manner described above. Furthermore, if Poiseuille flow is established inside the pore the streamline pattern must remain similar for all values of $L > \frac{1}{2}$ including the limiting case as $L \to \infty$. Hence, for $L > \frac{1}{2}$ the velocity profile at the exit of the pore is unchanged. Figure 6 shows the radial and axial velocity components at the pore exit in comparison to Poiseuille and Sampson profiles. An interesting result from this comparison is that the axial velocity at the exit of the pore can be computed from the arithmetic average of Poiseuille and Sampson profiles to four significant digits.

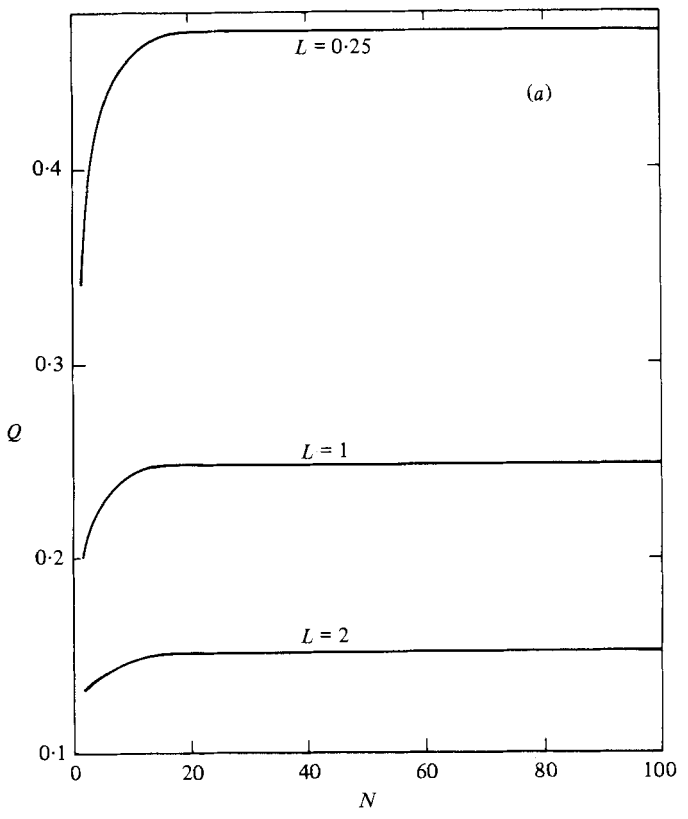

FIGURE 2. For legend see facing page.

The volumetric flow rate was calculated directly from the value of the stream function on the boundary. In general, one can express the relations between the pressure drop across the pore $\Delta P'$ and the volumetric flow rate Q' as follows:

$$\Delta P' = \Pi(L)\frac{Q'\mu}{a^3}, \tag{3.1}$$

where P' and Q' are dimensional variables, μ is the dynamic viscosity, a the pore radius and $\Pi(L)$ is a function of the aspect ratio L. For $L = 0$ Sampson obtained the result:

$$\Pi(0) = 3. \tag{3.2}$$

For other values of L, Π is shown in figure 7. Clearly, the behaviour suggests linear relations between the pressure drop and the aspect ratio. A simple approximate expression for the pressure drop can be obtained by assuming Poiseuille flow throughout the pore and Sampson's solution outside; then

$$\Pi(L) = 16L/\pi + 3. \tag{3.3}$$

The calculated values of $\Pi(L)$ were compared with equation (3.3) and are shown in table 1. The good agreement between the exact and the approximate value is not surprising since the actual flow field deviates from the assumed one only in the vicinity of the pore opening and even in this region the local axial velocity profile does not depart significantly from a parabolic distribution.

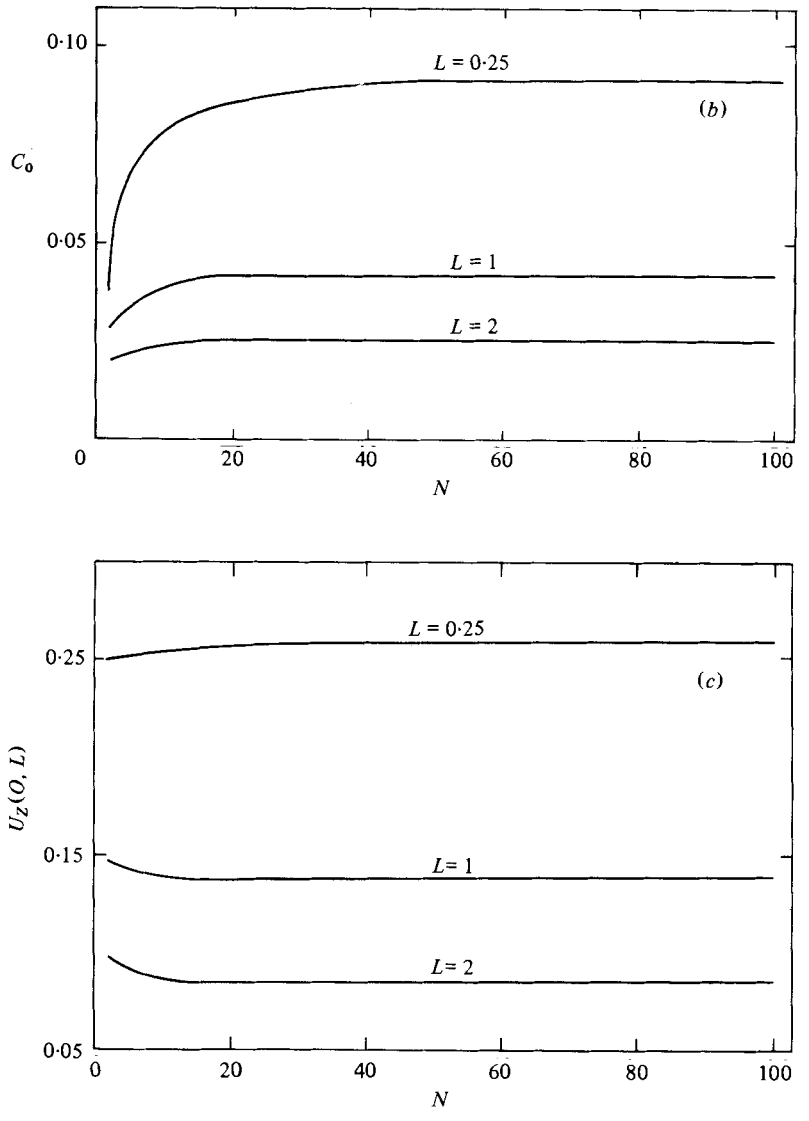

FIGURE 2. (*a*) Convergence test for the volumetric flow rate Q. (*b*) Convergence test for the constant C_0. (*c*) Convergence test for the exit centre-line velocity $U_Z(0, L)$.

4. Concluding remarks

The present solution for the flow through a finite-length pore suggests two general conclusions. First, the entrance effects are significant only near the pore opening, and decay to within 1·5 % of a Poiseuille profile at a distance of half the pore radius when $L > \frac{1}{2}$. Secondly, the pressure drop across an orifice of finite length can be closely approximated (less than 1 % error) by (3.1) and (3.3), which do not account for the upstream influence across the pore opening.

The method of solution used in the present problem can be easily applied to problems with boundaries that cannot be defined by a natural co-ordinate system. In

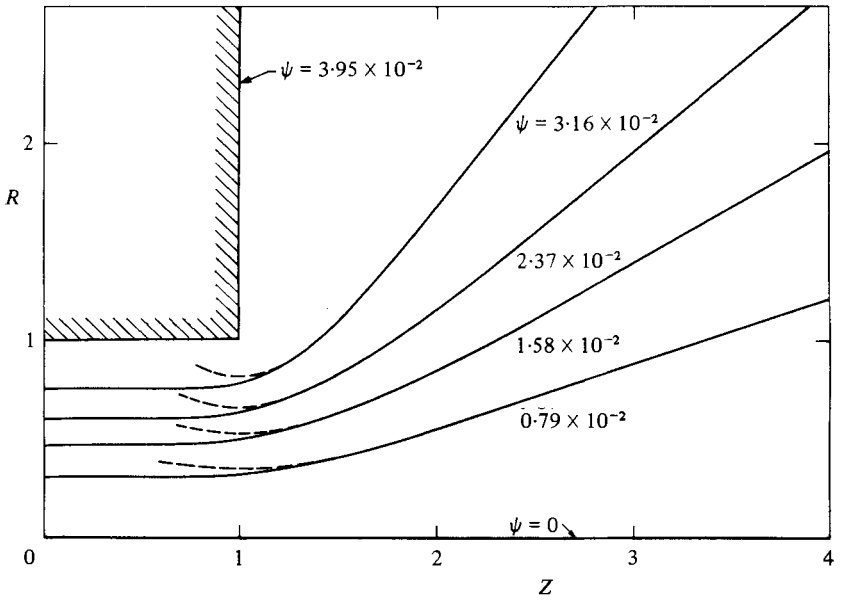

FIGURE 3. Streamline pattern for the flow through a pore of finite length with $L = 1$. ------, Sampson's (1891) solution for the flow through a zero-thickness orifice.

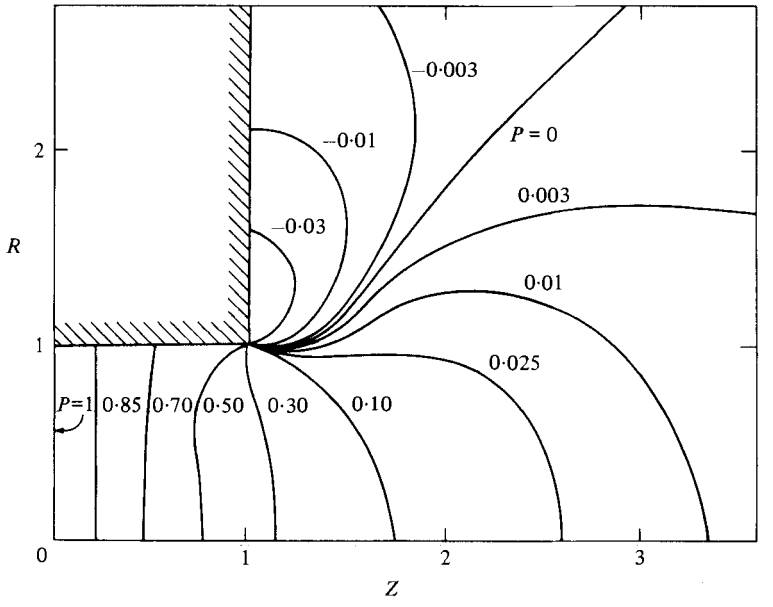

FIGURE 4. Pressure field for the flow through a pore of finite length with $L = 1$.

particular, the study of filtration through nuclepore filters is modelled simply by a periodic distribution of equally spaced pores with an outer boundary which is a cylindrical volume coaxial with the pore. Furthermore, by combining the application of the procedure outlined, together with the collocation technique described in detail in Ganatos *et al.* (1978), it is possible to study the motion of a sphere near boundaries of more complex shape. The interesting problem of the axisymmetric creeping

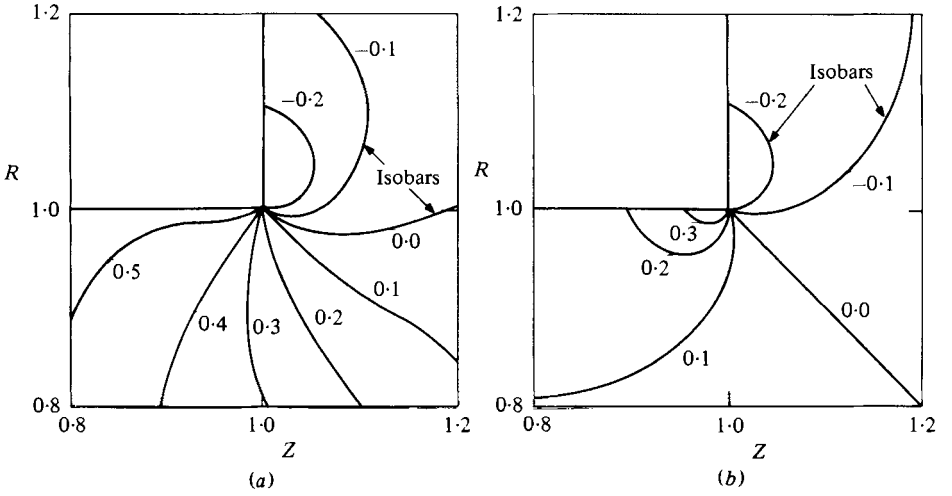

FIGURE 5. Comparison between (*a*) the pressure field near the edge of the orifice ($L = 1$) and (*b*) the locally valid two-dimensional pressure field in the vicinity of the trailing edge (Weinbaum 1968).

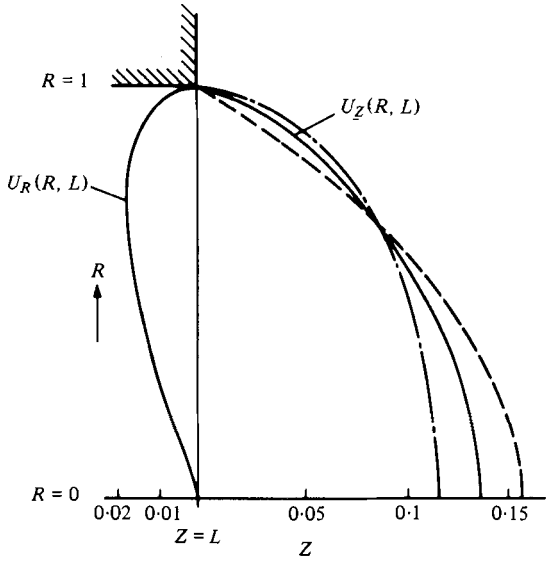

FIGURE 6. Radial and axial velocity profiles at the pore exit ($L = 1$). – – – –, Poiseuille profile; — · — ·, velocity profile at the opening of a zero-thickness orifice (Sampson 1891).

motion of a sphere towards a pore of finite length can be treated by using different stream-function representations for the finite pore and for the outer infinite half-space containing the sphere. Inside the pore, (2.6) is retained, while outside a superposition of the disturbances generated by the orifice wall and by the sphere yield:

$$\psi^{\mathrm{I}} = \psi_{\mathrm{w}} + \psi_{\mathrm{s}} \tag{4.1}$$

where ψ_{w} is given by (2.5) and ψ_{s} is the axisymmetric spherical solution of the Stokes equation given by Sampson (1891):

$$\psi_{\mathrm{s}} = \sum_{n=2}^{\infty} [C_n r^{-n+1} + D_n r^{-n+3}] I_n(\cos\theta). \tag{4.2}$$

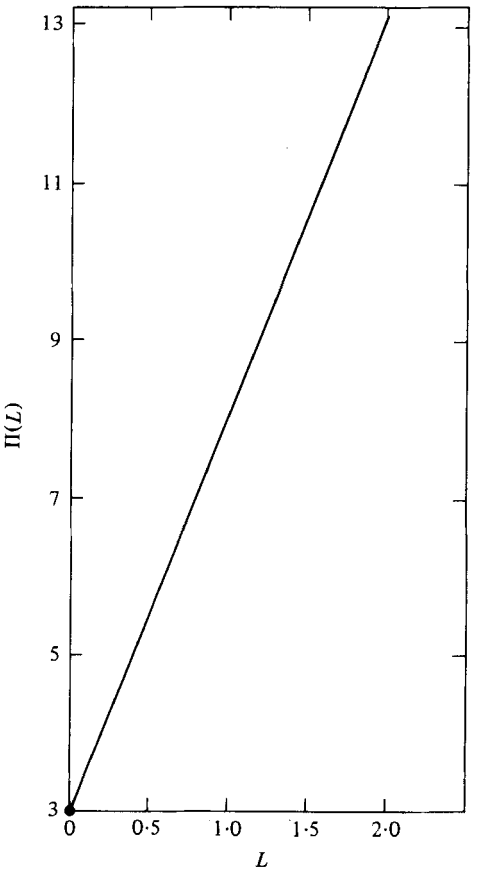

FIGURE 7. Behaviour of the function $\Pi(L)$. ●, Sampson (1891).

Aspect ratio L	$\Pi(L)$ Exact	(3.3)
0	3·00†	3·00
0·25	4·25	4·27
0·5	5·51	5·55
0·75	6·79	6·82
1·00	8·06	8·09
1·25	9·33	9·37
1·5	10·6	10·6
2·0	13·2	13·2

† Sampson (1891).

TABLE 1. Comparison of the approximate expression (3.3) with the exact solution for $\Pi(L)$

Here, (r, θ) are spherical co-ordinates, C_n and D_n are unknown constant coefficients and I_n are the Gegenbauer functions of order n and degree $-\frac{1}{2}$.

Using (2.7) for the exit-plane velocity representation the no-slip boundary conditions inside the pore can be applied in the manner shown in § 2. Outside the pore, the no-slip boundary conditions are applied with the use of the Hankel transform, yielding solutions for $A(\omega)$ and $B(\omega)$ in terms of the spherical coefficients C_n and D_n and the unknown velocity at the exit plane. The pressure-matching conditions at the interface between the two regions provide relations for the unknown constant coefficients in the series representation of the exit velocity in a form of an incomplete set of linear algebraic equations containing the constants C_n and D_n. To complete this set, the no-slip boundary conditions on the surface of the sphere are satisfied at M discrete points, providing an additional $2M$ equations for C_n and D_n to the set of linear algebraic equations, which can be solved by any matrix reduction technique.

The authors wish to thank the National Science Foundation for supporting this research under grant no. ENG78-22101 and the City University of New York Computer Center for the use of their facilities. The above work has been performed in partial fulfilment of the requirements for the Ph.D. degree of Z. Dagan from The School of Engineering of The City College of The City University of New York.

Appendix

This appendix contains a detailed description of the analytic evaluation of the integrals in (2.31). Substitution of $a^*(R)$ and $b^*(R)$ from (2.30) into (2.31) results in triple integrals, of which the inner and the outer are definite integrals, which can be easily evaluated leaving improper integrals of the form

$$A_{kn} = \int_0^\infty \frac{\omega J_1(\omega) J_0(\omega)}{(\omega^2 - \lambda_{n,1}^2)(\omega^2 - \lambda_{k,0}^2)} d\omega, \quad B_{kn} = A_{nk} - \frac{1}{\lambda_{k,0}^2} \int_0^\infty \frac{\omega J_1(\omega)}{\omega^2 - \lambda_{n,1}^2} d\omega, \quad \text{(A 1, 2)}$$

in (2.31a, b), respectively.

Using the result given by Oberhettinger (1972),

$$\int_0^\infty \frac{\omega J_1(\omega)}{\omega^2 - \lambda_{n,1}^2} d\omega = \tfrac{1}{2}\pi H_{-1}(\lambda_{n,1}), \tag{A 3}$$

where H_ν is the Struve function of order ν (for a discussion of the Struve function see Watson 1958). The recurrence relations

$$H_{\nu-1}(Z) + H_{\nu+1}(Z) = \frac{2\nu}{Z} H_\nu(Z) + \frac{(\frac{1}{2}Z)^\nu}{\sqrt{\pi}\,\Gamma(\nu+1)} \tag{A 4}$$

are used in (A 3) to replace the right-hand side with a Struve function of a positive order; then

$$\int_0^\infty \frac{\omega J_1(\omega)}{\omega^2 - \lambda_{n,1}^2} d\omega = 1 - \tfrac{1}{2}\pi H_1(\lambda_{n,1}).$$

To evaluate A_{kn}, we write

$$A_{kn} = \frac{1}{\lambda_{k,0}^2 - \lambda_{n,1}^2} [S(\lambda_{n,1}) - S(\lambda_{k,0})], \tag{A 5}$$

where

$$S(t) = \int_0^\infty \frac{\omega J_0(\omega) J_1(\omega)}{t^2 - \omega^2} d\omega, \tag{A 6}$$

and t must be a root of J_0 or J_1. Furthermore, $S(t)$ can be written as follows:

$$S(t) = \lim_{a\to 1} \frac{d}{da} \int_0^\infty \frac{J_0(\omega)\, J_0(\omega a)}{\omega^2 - t^2}\, d\omega. \tag{A 7}$$

From the addition theorem one can obtain the equation

$$J_0(\omega)\, J_0(\omega a) = \frac{1}{\pi} \int_0^\pi J_0(\omega(1 + a^2 - 2a\cos\theta)^{\frac{1}{2}})\, d\theta. \tag{A 8}$$

Substitution of (A 8) into (A 7) gives rise to an outer integral of the form given in Oberhettinger (1972), which can be evaluated. Differentiation with respect to a and setting $a = 1$ yields

$$S(t) = \frac{1}{2} \int_0^\pi \left[H_1(2t \sin \tfrac{1}{2}\theta) - \frac{2}{\pi} \right] \sin \tfrac{1}{2}\theta\, d\theta, \tag{A 9}$$

or with the substitution $\cos\theta = \mu$ it becomes

$$S(t) = \int_0^1 H_1(2t\sqrt{(1-\mu^2)})\, d\mu - \frac{2}{\pi}. \tag{A 10}$$

The integral in (A 10) can be determined by making use of the series representation of H_1 and term by term integration, then:

$$S(t) = \frac{16t^2}{9\pi}\, {}_2F_3(2, 1; \tfrac{3}{2}, \tfrac{5}{2}, \tfrac{5}{2}; -t^2) - \frac{2}{\pi} \tag{A 11}$$

where ${}_2F_3$ is the generalized hypergeometric series defined by

$${}_pF_q(\alpha_1, \alpha_2, \ldots, \alpha_p; \beta_1, \beta_2, \ldots, \beta_q; z) = \sum_{k=0}^{\infty} \frac{(\alpha_1)_k (\alpha_2)_k, \ldots, (\alpha_p)_k z^k}{(\beta_1)_k (\beta_2)_k \cdots (\beta_p)_k k!}, \tag{A 12a}$$

and

$$(a)_k = \Gamma(a+k)/\Gamma(a). \tag{A 12b}$$

The numerical evaluation of $S(t)$ can be accomplished by summing the series in (A 11) or by numerical integration of (A 10). The latter was found to be more efficient. The computation of H_1 in (A 10) was made possible by an expansion in series of Chebyshev polynomials given by Luke (1969). Although the integration is numerical, it does not prolong the overall computation time because $S(t)$ is independent of the characteristic lengths in the problem and can therefore be performed once for all possible values of L and N.

REFERENCES

Dagan, Z., Weinbaum, S. & Pfeffer, R. 1982 *J. Fluid Mech.* (in press).

Dean, W. R. & Montagnon, P. E. 1949 *Proc. Camb. Phil. Soc.* **45**, 389.

Fahraeus, R. 1929 *Physiol. Rev.* **9**, 241.

Fahraeus, R. & Lindqvist, T. 1931 *Am. J. Physiol.* **96**, 562.

Ganatos, P., Pfeffer, R. & Weinbaum, S. 1978 *J. Fluid Mech.* **84**, 79.

Ganatos, P., Pfeffer, R. & Weinbaum, S. 1980 *J. Fluid Mech.* **99**, 755.

Ganatos, P., Weinbaum, S. & Pfeffer, R. 1980 *J. Fluid Mech.* **99**, 739.

Gluckman, M. J., Pfeffer, R. & Weinbaum, S. 1971 *J. Fluid Mech.* **50**, 705.

Haberman, W. L. & Sayre, R. M. 1958 *David W. Taylor Model Basin Rep.* no. 1143. Washington, D.C.

Kanaoka, C., Emi, H. & Nskada, K. 1974 *Kagaku Kogaku* **38**, 223.

LEICHTBERG, S., PFEFFER, R. & WEINBAUM, S. 1976 *Int. J. Multi-phase Flow* **3**, 147.

LUGT, H. J. & SCHWIDERSKI, E. W. 1965 *Proc. R. Soc. Lond.* A **285**, 382.

LUKE, Y. L. 1969 *The Special Functions and their Approximation*, vol. 2. Academic.

MANTON, I. L. 1978 *Atmos. Environ.* **12**, 1669.

OBERHETTINGER, F. 1972 *Tables of Bessel Transforms*. Springer.

PARKER, R. D. & BUZZARD, G. H. 1978 *J. Aerosol. Sci.* **9**, 7.

PARMET, I. L. & SAIBEL, E. 1965 *Comm. Pure Appl. Math.* **18**, 17.

SAMPSON, R. A. 1891 *Phil. Trans. R. Soc. Lond.* A **182**, 449.

SKALAK, R., CHEN, P. H. & CHIEN, S. 1972 *Biorheol.* **9**, 449.

SMITH, T. N. & PHILLIPS, C. R. 1975 *Environ. Sci. Tech.* **9**, 564.

TRANTER, C. J. 1951 *Quart. J. Math.* **2** (2), 60.

WATSON, G. M. 1958 *A Treatise on the Theory of Bessel Functions*, 2nd edn. Cambridge University Press.

WEIL, H. & SCHENECTADY, N. Y. 1951 *J. Appl. Mech.* **18**, 267.

WEINBAUM, S. 1968 *J. Fluid Mech.* **33**, 38.

WEINBAUM, S. & CARO, C. C. 1976 *J. Fluid Mech.* **74**, 611.